NASA TECHNICAL MEMORANDUM

NASA TM -78837

NASA TM-78837

MEASUREMENT OF THE TIME-TEMPERATURE DEPENDENT DYNAMIC MECHANICAL PROPERTIES OF BORON/ALUMINUM COMPOSITES

by J. A. DiCarlo
Lewis Research Center
Cleveland, Ohio 44135

and

J. E. Maisel
Cleveland State University
Cleveland, Ohio 44115

TECHNICAL PAPER to be presented at the
Fifth Conference on Composite Materials: Testing and Design
sponsored by the American Society for Testing and Materials
New Orleans, Louisiana, March 20-23, 1978

MEASUREMENT OF THE TIME-TEMPERATURE DEPENDENT DYNAMIC MECHANICAL PROPERTIES OF BORON/ALUMINUM COMPOSITES

J. A. DiCarlo* and J. E. Maisel†

ABSTRACT

A flexural vibration test and associated equipment have been developed to accurately measure the low strain dynamic modulus and damping of composite materials from -200° C to over 500° C. The basic test method involves the forced vibration of composite bars at their resonant free-free flexural modes in a high vacuum cryostat-furnace. The complex modulus approach was employed to derive theoretical expressions for composite axial and transverse dynamic properties in terms of the dynamic properties of the constituent phases. The accuracy of these expressions and the flexural test was verified by dynamic moduli and damping capacity measurements on 50 fiber volume percent boron/aluminum (B/Al) composites vibrating near 2000 Hz. Whereas the properties of the highly anelastic fiber were measured on single fibers, the aluminum matrix properties were in most part deduced from the B/Al results. The phase results were summarized to permit predictions of the B/Al dynamic behavior as a function of frequency, temperature, and fiber volume fraction. Analysis of the test data has also indicated several areas in which B/Al dynamic properties might be exploited to evaluate and predict gross composite behavior as a function of environmental conditions encountered in fabri-

*Physicist, Material Science Branch, NASA Lewis Research Center, Cleveland, Ohio, 44135.

†Professor of Electrical Engineering, Cleveland State University, Cleveland, Ohio, 44115.

E-9548

STAR Category 24

cation and use. These areas include fiber-matrix debonding, fiber interaction with matrix and impurities, and thermal treatment effects on the matrix.

KEY WORDS: composite materials, flexural vibration test, dynamic modulus, damping, boron/aluminum composite, boron fiber, aluminum alloy matrix, thermal treatment

INTRODUCTION

The primary objective of this research was to develop a relatively simple test for accurately measuring the low strain dynamic properties of composite materials as a function of frequency (time) and temperature. Clearly the results of such a test can be of significant value in the design of structures subject to vibration. Upon achievement of this first goal, the next objective was to utilize the test data to verify the predictive accuracy of theoretical expressions for the composite dynamic properties. If these expressions which are based on the dynamic properties of the constituent phases could be verified for a large variation in a parameter such as temperature, composite dynamic response could then be predicted for conditions not included in the test. A third objective was to explore whether the test data could be used to yield basic information concerning environmental effects on the microstructure, macrostructure, and other physical properties of the composite and its constituent phases. If this information could be correlated with variations in macroscopic composite properties, the dynamic properties could then become a practical tool for evaluating and predicting composite mechanical behavior as a function of environmental conditions.

To achieve the above objectives, the low strain dynamic modulus and damping capacity of boron/aluminum (B/Al) composites were measured from -200° C to 400° C. The reasons for this choice of composite were many. First, B/Al is a metal matrix composite of current aerospace interest for which dynamic data would be useful for design purposes. Second, fabrication techniques for B/Al were fairly well established, thereby enhancing the probability of obtaining consistent microstructural and macrostructural properties. Third, from our previous work there existed accurate data concerning the low strain dynamic behavior of the modern boron fiber (1,2,3). Fourth, in contrast to the essentially elastic behavior of other reinforcement fibers, the boron fiber displays a large amount of anelasticity which is not only reproducible but also predictable in time and temperature. Fifth, much data were available in the literature concerning the time-temperature dependent dynamic properties of aluminum alloys. Finally, the possibility may exist that dynamic data could be employed to detect the growth of detrimental boron-aluminum interaction phases created by heat treating the composite above 500° C.

PROCEDURE

Apparatus

A simple flexural test was developed for measuring the low strain dynamic modulus and damping capacity of composite materials from -200° C to over 500° C. The basic test technique consisted of the forced flexural vibration of composite bars at their two lowest free-free symmetrical resonant modes in a high vacuum cryostat-furnace. The free-free configuration avoided the spurious clamp effects often encountered when massive

specimens are vibrated in the fixed-free cantilevered mode (4,5). As shown schematically in Fig. 1, support for the composite specimen was accomplished by two sets of adjustable stainless steel screw pins located at two vibrational nodes. Whereas the two pins of the upper set were threaded through a rigid support, the two pins of the lower set were threaded through a circular ring which itself was not fixed but only slip fitted into a hole in the lower rigid support. This was done in order to simplify specimen mounting and to minimize stresses caused by rotation and expansion of the composite during thermal cycling.

Before the mounting of each specimen, slight indentations for pin support were made at the theoretical nodal positions on the specimen side faces. For this the composite was assumed to be a rectangular parallelopiped symmetric across its thickness and to have a length to thickness ratio large enough to neglect transverse shear effects during vibration (6). As such, the first tone nodes are located at $h/2$ across the specimen thickness h and at 0.224ℓ and 0.776ℓ along the specimen length ℓ (7). Although four nodes exist for the third tone, for this work the nodal positions at $h/2$ and 0.094ℓ and 0.644ℓ were chosen so that the pin set separation was almost the same as that of the first tone. This permitted rapid specimen mounting for either tone without any movement of the two main rigid supports and only slight vertical translation of the circular ring support.

Vibration drive and detection was achieved electrostatically by two electrodes positioned at convenient vibrational antinodes. As shown in Fig. 1 these electrodes were simply stainless steel bolts with heads

machined flat to allow adjustment close to the composite surface. Typical gap separations ranged between 100 and 200 μm. Electrical insulation between the electrodes and the stainless steel main frame was provided by sapphire washers. These washers could be adjusted vertically within a slot in the main frame, thereby allowing electrode positioning at specimen antinodes.

A block diagram of the electrical drive and detection system is shown in Fig. 2. The specimen electrostatic drive force $F \cos \omega t$ was produced by an alternating voltage $V_{ac} \cos \omega t$ from the audio amplifier superimposed on a dc voltage V_1 provided by the variable high voltage supply. Because the drive electrode and specimen formed a parallel plate capacitor, the force amplitude was

$$F = \beta A_p V_1 V_{ac} / (g_1)^2 \tag{1}$$

Here $\beta = 8.9 \times 10^{-12}$ newtons/volt^2, A_p is the area of the capacitor plates, and g_1 is the gap separation between the drive electrode and specimen.

For detection, a high impedance operational amplifier was employed as a charge amplifier to measure any change $\Delta g_2 \cos \omega t$ in the gap separation g_2 between the detector electrode and the specimen. By application of a dc voltage V_2 (=300 volts) to the detector electrode, specimen displacement was converted to an alternating voltage $S \cos \omega t$. Under optimum gain conditions the amplitude of the output signal from the operational amplifier was

$$S = \frac{\Delta g_2}{g_2} V_2 \tag{2}$$

A lock-in amplifier was used to further amplify this signal and to eliminate extraneous off-frequency noise. It is estimated that this detection system can sense specimen displacements as low as one nanometer.

For dynamic measurements as a function of temperature, the stainless steel main frame (Fig. 1) was hung vertically by thin wires in a long cylindrical vacuum chamber. The wires (5 mil tantalum) isolated the main frame both thermally and vibrationally. To further reduce external noise, vacuum conditions were maintained by an ion pump at pressures below 10^{-7} torr. A metallic shield was placed between the electrode and around the main frame in order to reduce pickup of the drive signal at the detection electrode and to minimize thermal gradients during temperature cycling. For temperature measurement thin gage chromel-alumel thermocouple wires were attached to the main frame. To achieve temperatures above 22° C, the vacuum chamber was inserted in the 7.6 cm bore of a resistance-heated furnace. Warmup and cooldown rates were kept low ($\sim$2° C/min) in order to minimize thermal gradients. For measurements between -200 and 22° C, the vacuum chamber was filled with dry nitrogen gas and then inserted into a liquid nitrogen bath. When temperatures near -200° C were reached, the nitrogen gas was pumped out and the nitrogen bath removed, allowing the main frame to warmup slowly to 22° C ($\sim$6 hours).

Dynamic Measurements

For determination of the flexural dynamic modulus E^b as a function of temperature T, the forced resonance method was employed in which the variable drive oscillator was manually tuned to that frequency which

produced maximum vibrational displacement. For the free-free flexural modes of bar specimens with low damping, these resonant (angular) frequencies $\omega_n(T)$ are related to E^b by

$$\omega_n^2 = b_n^2 \left[\frac{w}{m}\left(\frac{h}{\ell}\right)^3\right] E^b \qquad (3)$$

where m, h, w, and ℓ are the specimen mass, thickness, width, and length, respectively (7). The frequency constant b_n depends on the tone number n and also on specimen dimensions if $\ell/h < 100$ (rotary inertia and shear deformation effects). Simplified formulas to calculate accurate b_1 and b_3 values for $\ell/h < 100$ have been derived in Appendix I using Huang's transcendental equation for free-free boundary conditions (6). From Eq. 3 it is seen that frequency can be varied by changing tones or specimen dimensions.

Besides being temperature dependent, E^b was also frequency dependent due to the existence of time-dependent anelastic mechanisms within the specimen. During vibration the anelastic strains from these mechanisms gave rise to a total strain amplitude ε which lagged the stress amplitude σ by a phase angle $\phi(\omega,T)$. Thus specimen anelasticity produced both hysteretic or damping effects and a dynamic modulus less than the elastic flexural modulus $E^b(\omega = \infty)$. In this work specimen damping was determined from oscilloscope photographs of the free decay obtained after simultaneously removing the resonant drive signal and grounding the drive electrode. Because all data were taken at low strain amplitudes where the decay time constants were amplitude independent (linear anelasticity), it followed that proper expressions for the specimen damping capacity ψ were

$$\psi \equiv \frac{\Delta W}{W} = 2\pi \tan \phi = \frac{4\pi \ln (S_1/S_2)}{\omega(t_2 - t_1)} \qquad (4)$$

Here $\Delta W/W$ is the relative amount of stored energy lost per cycle, and S_1 and S_2 are the detector envelope signals at times t_1 and t_2, respectively. The more rapid free decay method was chosen over other damping measurement methods (7) because it was the least affected by detection problems caused by thermally-induced changes in the electrode gap separations and in the specimen damping ($\phi < 0.1$).

An alternate approach often used to express anelasticity effects on mechanical vibration is the concept of complex modulus E^* defined by

$$\sigma e^{i(\omega t+\phi)} = E^* \varepsilon e^{i\omega t} \qquad (5)$$

where

$$E^* = E^R + iE^I \qquad (6)$$

The real part E^R and the imaginary part E^I of E^* are referred to as the storage and loss modulus, respectively. It can be shown (7) that E^R is equivalent to the dynamic modulus E^b as measured from the resonant frequency ω_n and that

$$E^I = E^R \tan \phi = E^b \psi/2\pi \qquad (7)$$

It should be pointed out that for forced resonance, the frequency ω at maximum displacement is less than ω_n by a factor $[1 - (\tan \phi)^2/2]^{1/2}$. For this study ϕ was less than 0.02 so that this frequency correction could be neglected in the E^b calculations.

Composite Theory

For the unidirectional composite with fibers aligned within the plane of flexural vibration (axial mode), the flexural dynamic modulus

E^b is in general less than E_{11}, the tensile modulus for uniaxial extension parallel to the fiber direction. This difference is due primarily to a higher than average matrix volume fraction near the specimen bend surfaces. Appendix II analyzes this effect and shows that as the ply number N increases, the composite E^b rapidly approaches E_{11}. Likewise, for a unidirectional composite with fibers aligned perpendicular to the flexural vibration (transverse mode), a similar type of analysis (8) indicates that for large N the flexural E^b becomes essentially equal to E_{22}, the tensile modulus for uniaxial extension perpendicular to the fiber direction. Regarding the 8-ply B/Al composites of this study, the above results suggest that specimen flexural moduli were indeed less than the tensile moduli but by less than 0.6 percent. Because of this small difference, it was generally assumed for the purpose of data analysis that E^b measurements for the axial and transverse modes were in fact dynamic measurements of E_{11} and E_{22}, respectively.

To predict composite dynamic behavior in terms of fiber and matrix anelasticity, one can employ the complex modulus concept in the manner described by Hashin (9). In this approach the effective complex moduli of an anelastic (or viscoelastic) composite can be determined directly from the equations for composite effective elastic moduli by simply replacing the elastic moduli of the phases by their complex moduli. For instance, for unidirectional composites extended in the axial mode, the rule-of-mixtures (ROM) can be employed to predict the elastic modulus E^e_{11}. If anelastic effects are present, it follows that the composite complex modulus E^*_{11} is given by

$$E^*_{11} = v_f E^*_f + v_m E^*_m \tag{8}$$

where v is volume fraction, E^* is complex Young's modulus in the fiber direction, and the subscripts f and m refer to the fiber and matrix phase, respectively. The real parts of Eq. (8) yield the axial dynamic modulus

$$E_{11} = v_f E_f + v_m E_m; \tag{9}$$

whereas the imaginary parts yield the axial damping capacity

$$\psi_{11} = v_f \left(\frac{E_f}{E_{11}}\right) \psi_f + v_m \left(\frac{E_m}{E_{11}}\right) \psi_m \tag{10}$$

For unidirectional composites extended in the transverse mode, the theoretical expression for the elastic modulus E_{22} is quite complicated (9). For this reason we have employed the approximate Halpin-Tsai (HT) equation which has been found to predict E_{22} values in good agreement with the E_{22} derived from formal elasticity theory (10). Thus the complex modulus for the transverse mode can be expressed as

$$E^*_{22} = E^*_m \frac{(1 + \zeta \eta^* v_f)}{(1 - \eta^* v_f)} \tag{11}$$

where

$$\eta = (E^*_f - E^*_m)/(E^*_f + \zeta E^*_m) \tag{12}$$

The ζ parameter is a measure of reinforcement which depends on the boundary conditions (10). Under the assumption of low damping and deformation isotropy for the two phases, it follows that the transverse dynamic modulus should be predictable from

$$E_{22} = E_m[H/J] \tag{13}$$

where

$$H = (1 + \zeta v_f)E_f + (\zeta v_m)E_m \tag{14}$$

and

$$J = v_m E_f + (\zeta + v_f)E_m \tag{15}$$

Likewise for the transverse damping capacity, one should expect

$$\psi_{22} = (\gamma_{22})\psi_f + (1 - \gamma_{22})\psi_m \tag{16}$$

where

$$\gamma_{22} = v_f(1 + \zeta)^2 E_f E_m / HJ \tag{17}$$

Clearly the composite expressions for modulus and damping capacity are the baseline behavior to be expected from the fiber and matrix intrinsic properties. There could exist, however, other sources of anelasticity that are specific to composite structure, such as the fiber-matrix interface and fiber-matrix interaction phases. These additional mechanisms will reduce the composite dynamic modulus and increase damping in certain frequency and temperature ranges. It is therefore necessary to take extra care when comparing dynamic data with predictive theory because slight differences could be of practical significance for evaluating composite structure.

Specimens

The B/Al specimens for this research were obtained from 8-ply unidirectional panels containing nominally 50 volume percent fiber. The fibers were 203 μm (8 mil) boron on tungsten fibers commercially supplied by Avco; the matrix material was either 1100 or 6061 aluminum alloy. The diffusion bonded panels were fabricated by two manufacturers, hereafter

referred to as M1 and M2. Exact conditions during bonding were not available. Dynamic test specimens were diamond cut from the panels into nearly exact rectangular parallelpipeds with nominal dimensions of 2×11×102 mm. Four M1 axial mode specimens were supplied directly by the manufacturer; whereas one axial and one transverse mode specimen were cut in-house from the same M2 panel (6061 matrix). Tensile strength data for coupons obtained from the M1 and M2 panels have been reported elsewhere (11,12).

RESULTS

For this particular study of B/Al dynamic properties, temperature was the principal variable with frequency, strain amplitude, and fiber volume fraction held essentially constant. The frequency which was determined by the lowest free-free flexural resonant condition varied between 1700 and 2000 Hz for the axial specimens and was about 1400 Hz for the transverse specimen. Strain amplitudes at the specimen bend surfaces were kept below 10^{-6}. For this strain range the composite dynamic modulus and damping capacity were independent of vibrational amplitude (linear anelasticity).

Dynamic Moduli at 22° C

The room temperature property results for the axial and transverse B/Al specimens are listed in Table 1. Measurements of specimen mass, dimensions, and resonant frequency were employed to determine average fiber volume fraction v_f, average matrix density ρ_m, and the dynamic tensile modulus E_{11} or E_{22}. The v_f were calculated from

$$v_f = N_f \pi d^2/4wh \qquad (18)$$

where the fiber number N_f was determined optically and the fiber

diameter d was assumed to be 202.5±0.7 μm (3). The ρ_m values were calculated from

$$\rho_m = (\rho_c - \rho_f v_f)/v_m \tag{19}$$

where ρ_c is the measured composite density and ρ_f is the 203 μm boron fiber density measured to be 2.410 g/cm^3 (3). Because absolute values of E_{11} and E_{22} were required for data analysis, a small correction of +0.6 percent was applied to the flexural moduli E^b calculated from Eq. (3) (see Appendix II).

To verify the accuracy of the theoretical composite relations, the dynamic modulus to be expected for each specimen was calculated using the ROM Equation (9) for E_{11} and the HT Equation (13) for E_{22}. For the E_{11} calculation a very small correction (+1 GPa) was included to account for the Poisson's ratio difference between fiber and matrix (9). For the E_{22} calculation it was assumed that $\zeta = 2$ because of the nearly square array of fibers in the B/Al specimens (10). The phase properties and their literature sources are listed in Table 2. It should be pointed out that the Table 2 value for E_m is probably an overestimate because it neglects the unknown degradation effects of matrix anelasticity and matrix porosity (2 to 3 %). The theoretical moduli using the above parameters and the measured v_f are given in the last column of Table 1.

Examination of the Table 1 data indicates that the axial moduli E_{11} for the M1 specimens were not only very consistent and independent of matrix alloy but also in very good agreement with the ROM predictions. This finding supports the accuracy of both the flexural test and the ROM equation for dynamic axial moduli. On the other hand, the specimens

taken from the same M2 composite panel displayed E_{11} and E_{22} moduli measurably lower than the theoretical predictions. These results suggest that a physical condition necessary for application of the predictive relations existed in the M1 panels but was somehow lacking in the M2 panel. This problem became even more severe during thermal cycling. For example, the M2 E_{11} dropped by 5 percent after only one cycle between 22 and 450° C; whereas the E_{11} of a M1 6061 specimen decreased less than 1 percent after six cycles. Additional evidence for the M2 composite problem can be found in the fact that average 22° C ultimate tensile strength for coupons from the as-fabricated M1 and M2 panels were 1.6 GPa and 1.1 GPa, respectively (11,12).

At the present time it is not clear what the exact physical sources were for the degraded behavior of the M2 composite panel used in this study. Optical observations did not reveal any external problems nor any dissimilarities between the M1 and M2 specimens. Differences in matrix moduli may have existed due to, for example, differences in porosity. However, the similar density results of Table 1 do not support this interpretation. It appears then, by a process of elimination, that the problems of this particular M2 panel were somehow associated with incomplete fiber-matrix bonding. Although there was no direct experimental evidence for this conclusion, the absence of complete stress-strain transfer between fiber and matrix could certainly explain the observation of moduli and strength data lower than those of the "well-bonded" M1 specimens. Likewise, expansion stresses developed during thermal cycling might be expected to increase debonding if the original bonds

were weak. Along these lines, it should be pointed out that the transverse M2 specimen showed less than 1 percent change in E_{22} after two cycles above 450° C. This absence of thermal cycling effects may possibly be explained by E_{22} being fairly insensitive to fiber-matrix bonding and/or by smaller thermal expansion stresses because the transverse fiber lengths were a factor of 10 shorter than the axial fiber lengths.

Dynamic Moduli vs. Temperature

To express the temperature dependence of the dynamic moduli, it is convenient to employ the concept of relative modulus R_x defined as $E_x(T)/E_x^o$ where $E_x^o = E_x(22° C)$. The property $R_x(T)$ can be measured quite accurately because it eliminates many of the dimensional errors inherent in the absolute measurements of the room temperature modulus E_x^o. Thus, R_{11} for the axial mode can be determined from Eq. (3); i.e.,

$$R_{11} \equiv \frac{E_{11}(T)}{E_{11}^o} = \left[\frac{\omega(T)}{\omega(22° C)}\right]^2 \frac{(1 + \alpha_{11}\,\Delta T)^3}{(1 + \alpha_{22}\,\Delta T)^4} \qquad (20)$$

where $\Delta T = T - 22° C$ and α_{11} and α_{22} are the average coefficients for composite axial and transverse thermal expansion, respectively. Likewise from Eq. (3) the transverse mode R_{22} is given by

$$R_{22} \equiv \frac{E_{22}(T)}{E_{22}^o} = \left[\frac{\omega(T)}{\omega(22° C)}\right]^2 \frac{1}{(1 + \alpha_{11}\,\Delta T)} \qquad (21)$$

From the B/Al results of Kreider and Patarini (14), the expansion coefficients for a 6061 matrix were taken as $\alpha_{11} = 5.5\times10^{-6}/°C$ and

$\alpha_{22} = 19\times10^{-6}/°C$. As expected, the R_{11} data from the M1 axial composites showed little variation among specimens. The average M1 R_{11} results are shown in Fig. 3 together with the R_{22} data for the one M2 transverse specimen employed in this study. For clarity, data points taken about every 10° C are not shown. As previously mentioned, despite problems with the M2 R_{11} results, the M2 R_{22} data were reproducible during thermal cycling.

To apply composite theory to the temperature dependent axial results, one can write the ROM Eq. (9) in terms of R parameters, i.e.,

$$R_{11} = \frac{(v_f R_f)E_f^o + (v_m R_m)E_m^o}{v_f^o E_f^o + v_m^o E_m^o} \tag{22}$$

Here the temperature dependent terms are in parenthesis and the superscript o refers to the 22° C values. From Eq. (18),

$$v_f(T) = v_f^o[1 - \chi(T)] \tag{23}$$

where

$$\chi(T) = 2\,\Delta T(\alpha_{22} - \alpha_{11}) \tag{24}$$

Thus, even if the fiber and matrix moduli have no temperature dependence, (i.e., $R_f = R_m = 1$), the composite R_{11} will vary because of a changing fiber volume fraction. From the average room temperature results for the M1 specimens, Eq. (22) becomes

$$R_{11} = 0.864R_f(1 - \chi) + 0.136R_m(1 + \chi) \tag{25}$$

The R_f data measured for boron fibers vibrating near 2000 Hz are shown in Fig. 4. Regarding R_m data for the 6061 matrix it was decided that since the accuracy of the ROM theory had been proven at 22° C, it could

be employed at other temperatures to accurately determine R_m for the actual matrix material. The R_m results determined from Eq. (25), the R_{11} data of Fig. 3, and the R_f data of Fig. 4 are shown by the open circles of Fig. 4.

Examination of Eq. (25) indicates that the R_m contribution to the axial R_{11} is small in comparison to the R_f contribution. The R_m calculations from this equation are thus very sensitive to errors in fiber volume fraction. This is not the case, however, for R_m determinations from transverse R_{22} data in which matrix effects predominate. This can be shown by inserting the experimental R_{22} and R_f data into the HT Eq. (13) with $\zeta = 2$. The calculated R_m for the M2 6061 matrix are given in Fig. 4 for the fiber volume fraction range $40\ \% < v_f < 47\ \%$. The upper limit is the observed v_f and the lower limit is that v_f value required in the HT equation to yield the low E_{22} measurement. Thus, although fiber volume fraction was allowed to vary 7 percentage points, the calculated R_m varied only slightly. The agreement of this transverse R_m curve and the axial R_m points suggests that the dynamic moduli of the M2 and M1 6061 matrices show negligible difference in their temperature dependence. This can be explained by the fact that the Fig. 4 R_m results essentially represent the basic behavior of the 6061 elastic modulus with differences in anelastic effects being so small as to be unobservable. Although these R_m results might also suggest the validity of the HT theory, the v_f insensitivity of the transverse R_m make this conclusion somewhat tentative.

Axial Damping Capacity

The ROM Eq. (10) for axial damping capacity ψ_{11} indicates that for the average M1 axial specimen, the relative phase contributions are the same as those in the R_{11} Eq. (25). This being the case, it is important first to understand the temperature dependence of the controlling fiber damping and how it might be altered by environmental conditions within the composite.

For the temperature range -200° to +200° C, fig. 5a gives typical ψ_f curves for a 203 μm boron on tungsten fiber vibrating in flexure near 2000 Hz. Data points which were taken about every 10° C are not shown because they fell within 5 percent of the continuous curves. The top curve is for the as-received fiber, whereas the middle and bottom curves were measured after 90 minute heat treatments at 400° C in vacuum and in air, respectively. The decrease in ψ_f with heat treatment is tentatively explained by the reduction in fiber anelasticity due to the motion of atomic defects. For the vacuum treatment the defects might be identified as either intrinsic defects or surface impurities which migrate between 100 and 300° C. Apparently because of the rapid quench after fiber formation by chemical vapor deposition, these defects had not reached their final lattice position within the as-received fiber. After the 400° C vacuum treatment, the middle ψ_f curve remained stable for vacuum treatments up to 1100° C. For the air treatment the defects were presumably oxygen atoms which begin to react with boron near 400° C (15). In contrast to the vacuum results, the lower ψ_f curve might be expected to decrease further as the temperature of the air treatment is increased above

400° C, thereby allowing oxygen atoms to diffuse deeper into the fiber.

With this background, let us now examine the low temperature ψ_{11} results shown in Fig. 5b for a typical M1 6061 axial specimen. The top curve was measured for the as-fabricated condition and the bottom curve after a 30 minute heat treatment at 400° C in vacuum. For all composite heat treatments, the specimen remained supported in the flexural test apparatus. After the 400° C treatment, the ψ_{11} curve below 150° C remained stable even after a 30 minute vacuum treatment at 550° C. In comparing the as-fabricated ψ_{11} data with the ψ_f results, it must be realized that because of composite fabrication conditions (about 30 minutes near 500° C) the appropriate ψ_f curve would not be the as-received curve. More likely, the ψ_f curve for the fibers within the as-fabricated composite would be equal to or lower than the ψ_f vacuum treatment curve because impurity atoms such as oxygen existed near the fiber surfaces during diffusion bonding of the matrix material. The dropoff with vacuum treatment indicates that impurity effects on fiber behavior did not saturate during composite fabrication. However, the observed saturation after the 400° C treatment suggests that the Fig. 6b bottom curve for ψ_{11} represents the baseline behavior to be expected for 50 volume percent B/Al composites vibrating near 2000 Hz.

The above discussion clearly indicates that the fiber ψ_f and consequently the ψ_{11} are measurably dependent on environmental conditions at the fiber surface during composite fabrication and use. Because these conditions were unknown, it is difficult to verify the damping capacity Eq. (10) in terms of phase properties. However, from Fig. 5 it

should be obvious that the composite ψ_{11} reproduces almost exactly the relative structure observed in the single fiber ψ_f. Thus if matrix effects are present, ψ_m for the TRW 6061 matrix must be small (less than 0.5 %) and relatively structureless. This conclusion also implies that other damping sources contained in the low temperature measurements are negligible. These include both intrinsic sources such as those due to composite structure, interaction phases, and thermoelastic effects (7) and extrinsic sources such as those due to experimental problems in the flexural test and detection system. In addition, the close agreement between ψ_{11} and ψ_f supports the inherent assumption that boron fiber damping is the same for flexural and axial vibrations (within the composite).

Regarding damping capacity at high temperature, the stable ψ_f results of Fig. 6a were measured for a boron fiber after vacuum heat treatment at 400° C. Above 200° C the fiber anelasticity increases significantly reaching a peak value of 24 percent near 650° C and 2000 Hz. This effect is clearly seen in Fig. 6b which presents ψ_{11} for a typical M1 6061 axial specimen. The solid and dashed curves represent data, respectively, for the as-fabricated condition and for the condition after vacuum heat treatment for 30 minutes at 550° C. The heat treatment conditions were chosen in order to insure enough reaction between the aluminum matrix and the boron fiber to significantly degrade composite tensile strength (16). The objective here was to determine whether the ψ measurement could detect fiber degradation perhaps through detection of the boron-aluminum interaction phase. Also included in Fig. 6b are

the ψ_{11} results for the M2 6061 axial specimen in the as-fabricated condition.

Examination of Figs. 6a and 6b shows that before heat treatment the ψ_{11} of the M1 specimen was primarily controlled by the ψ_f expected for the fibers. In contrast to Fig. 5a, small decreases in ψ_f due to impurities are not discernable at high temperature. After the 550° C heat treatment, however, a new damping peak near 270° C is observed in the M1 data. From the M2 data it can be seen that this peak already existed in the as-fabricated M2 panel. At first glance these results might suggest that the damping structure is somehow associated with the thermally induced boron-aluminum interaction phase which is known to be detrimental to composite strength. Such a model could then explain the weakness of the M2 panel as being due to a fiber-matrix interaction caused by overprocessing during fabrication. However, although the verdict on this tempting model is not yet final, it would appear from the following transverse mode results that the heat treatment peak is specific to the matrix and not to any new phase created within the composite.

Transverse Damping Capacity

The ψ_{22} damping capacity curve presented in Fig. 7a was measured for the M2 transverse specimen in the as-fabricated condition. Comparing this curve with the ψ_{11} results of Figs. 5b and 6b, one finds at any given temperature only small quantitative differences in the structureless background damping. The only significant dissimilarity concerns the peak structure near 270° C which is measurably larger in the M2 ψ_{22} data than in the M2 ψ_{11} data and does not appear at all in the as-fabricated M1 ψ_{11} data.

Although analytical experimental studies to firmly establish the phase microstructure responsible for this peak have yet to be performed, the application of composite theory to the damping results has shed some light on the most likely phase to examine. From the data concerning the 270° C peak, one must conclude that high temperature treatment of a B/6061 Al composite somehow creates a new anelastic mechanism within the composite structure. This mechanism may be located in the boron fiber, in the aluminum alloy, or possibly in the new phase created by the boron-aluminum interaction. For the specimens from the M2 panel, the damping capacity Eqs. (10) and (16) together with the Table 1 moduli predict that

$$\psi_{11} = 0.82\ \psi_f + 0.18\ \psi_m \tag{26}$$

and

$$\psi_{22} = 0.31\ \psi_f + 0.69\ \psi_m \tag{27}$$

Clearly these relations eliminate the fiber phase from consideration because if a change $\Delta\psi_f$ in the fiber damping had occurred near 270° C, the peak height $\Delta\psi_{11}$ would have been greater than the peak height $\Delta\psi_{22}$. In addition, the interaction phase can be ruled out not only because of its small volume fraction but also because if it is assumed to have a modulus similar to that of the fiber, its damping contribution can be considered part of $\Delta\psi_f$. It appears then that peaks in ψ_{11} and ψ_{22} are best explained by an increase in ψ_m. Using Eq. (27) with the ψ_f and ψ_{22} data, one can calculate the solid curve shown in Fig. 7b for the ψ_m damping capacity of the 6061 matrix in the M2 transverse specimen. For comparison purposes, this figure also includes the 800 Hz data measured

by G. Rieu for a 6061 bulk specimen (17).

Examination of Fig. 7b shows that even if the heat treatment peak were not present, the background damping of the 6061 aluminum alloy would like that of the fiber increase significantly above 200° C. Using the dashed line estimated from the bulk data, one finds a peak height $\Delta\psi_m$ = 5.3 percent for the anelastic mechanism in the M2 panel. This result inserted in Eq. (27) predicts that $\Delta\psi_{11}$ = 1.1 percent, a value in good agreement with the Fig. 6b peak heights for both the M2 and the heat-treated M1 axial specimens. Thus examination of the damping data in light of composite theory suggests that the temperatures employed to fabricate the M2 panel were high enough to produce within the 6061 microstructure an anelastic process which displays at ∿2000 Hz a damping peak near 270° C. A search of the literature suggests that this peak may be similar to that observed by Williams (18). Whether the peak's existence is an indication of some form of B/Al property degradation has yet to be determined.

DISCUSSION

The Flexural Test

The flexural vibration test has achieved the prime objective of this research which was to develop a relatively simple test to accurately measure as a function of temperature the low strain dynamic response of composite materials. Specimen preparation required prior to mounting was minimal consisting of only minor mechanical work to assure parallel faces and to locate indentations for pin support. The use of pins to support the specimen at intrinsic vibrational nodes eliminated the spurious frequency and damping effects often encountered whenever a vibrational node

of a relatively massive specimen has to be maintained by external clamps. From the close agreement of the B/Al dynamic modulus and damping capacity with composite theory, it is estimated that damping capacity contribution of the pins was less than 0.01 percent. Allowing one set of pins to translate and rotate in-situ not only assured that these pin effects remained negligible during thermal cycling but also simplified specimen mounting for the two lowest symmetrical free-free modes.

For this particular B/Al study all dynamic measurements were made at the first tone resonant frequency. One reason for this was that the frequency dependent dynamic properties of the two constituent phases were well documented. Thus, when composite theory was found applicable at one frequency, composite dynamic properties could be predicted for all frequencies (see next section). A second reason for employing the lowest mode was that it minimized the effect of an experimental limitation on the electrostatic drive force. Due to possible electrical breakdown of components within the drive system, the upper limits for the dc and ac drive voltages were about 1000 and 500 volts, respectively. Assuming the drive force to be concentrated at one point on the specimen, it can be shown from energy considerations that at forced resonance the displacement amplitude of that point is given by

$$\Delta g_1 = 8\pi F/m\omega^2\psi \tag{28}$$

It follows then from Eq. (1) that with $g_1 = 100$ μm, $A_p = 1$ cm^2, and $m = 6$ gm, maximum displacement based on upper limit voltages was

$$\Delta g_1 \simeq \frac{200}{\omega^2\psi} \ (m \cdot sec^{-2}) \tag{29}$$

From this it can be seen that higher vibrational displacements and thus better signal-to-noise ratios were available at the first tone frequencies. For the B/Al composites this became especially important at high temperatures where both ψ_{11} and ψ_{22} reached significantly high values.

Regarding the measurement of dynamic properties as a function of strain, the highest strain amplitude available in the flexural test was again dictated by the electrostatic drive technique. For symmetric free-free vibrations at tone n, the maximum strain amplitude at the surface of the specimen midpoint is given by

$$\varepsilon^{max} = C_n h \, \Delta g_1 / \ell^2 \tag{30}$$

where $c_1 = 8.88$, $c_3 = 42.5$, and Δg_1 is free end vibrational amplitude. Since the drive force was exerted at the free end, it follows from Eq. (29) that the highest ε^{max} available for the B/Al specimens at room temperature was about 4×10^{-4}. Thus the electrostatic drive was not strong enough to achieve strains where plastic or new anelastic effects become apparent (3). At these higher strains, the flexural test would not only require a different force method but also a different method of measuring damping since the free decay envelope would no longer be exponential in time.

Composite Dynamic Theory

Whenever possible, the measured axial and transverse dynamic properties of the B/Al specimens were used to verify the predictive accuracy of composite theory. The theoretical expressions given in Eqs. (9), (10), (13), and (16) were developed by replacing the phase elastic moduli with phase complex moduli in the rule-of-mixtures axial modulus and the Halpin-Tsai transverse modulus equations. Of the three independent

variables contained in these expressions, only temperature was allowed to change from -200 to over 400° C. The fiber volume fraction and the composite vibrational frequency were kept essentially constant at 50 percent and 2000 Hz, respectively. This approach to verify composite theory can be contrasted with that of other experimental work in which only room temperature elastic moduli were measured as fiber volume fraction was varied. The major new element provided by this study was thus the inclusion of the complex modulus concept and its verification through sensitive damping measurements. The phase damping was provided not only by the aluminum matrix but also by the highly anelastic boron fiber.

As pointed out in the presentation of the results, exact verification of the dynamic relations for composite damping was difficult because of slight variations in the phase properties due in the most part to different fabrication techniques of the two manufacturers. This was especially true for the anelastic properties of the aluminum matrices. To eliminate this problem the ideal experiment would have been to measure the damping of an axial and transverse specimen obtained from the same composite panel. The agreement in the matrix contributions as derived from two independent dynamic relations would then confirm the validity of both relations. Unfortunately, because of bonding problems in the M2 panel this approach could not be implemented in this particular B/Al study. Nevertheless, certain aspects of the dynamic moduli and damping data can be employed to make some general conclusions concerning the predictive accuracy of the composite theory.

For axial data the matrix contributions were relatively small in comparison to that of the fiber so that slight deviations in matrix properties were essentially unobservable. Thus the ROM prediction for the 22° C dynamic axial modulus was found to give good agreement with the M1 experimental E_{11} for both 6061 and 1100 matrices. This result can be contrasted with the poor agreement between ROM prediction and the measured M2 E_{11} which must be interpreted as a deficiency in the M2 panel rather than in the theory. Regarding damping data in support of ROM theory, the axial results of Figs. 5 and 6 show good quantitative and very good qualitative agreement between the fiber damping ψ_f and the M1 ψ_{11}. Exact verification is impossible here because manufacturing effects on ψ_f and the matrix damping ψ_m were unknown.

To obtain an approximate idea of the dynamic behavior of the 6061 matrix, one can examine the dynamic data for the M2 transverse specimen. Admittedly the low E_{11} and E_{22} data of Table 1 imply that the M2 panel results should not be employed for absolute quantitative analysis. However, the reproducibility of the transverse data coupled with the insensitivity of the HT equation to fiber volume fraction suggest that relative behavior of the 6061 matrix can be extracted. This is confirmed in Fig. 4 where the R_m calculated from the ROM equation and the M1 R_{11} show good agreement with the R_m calculated from the HT equation and the M2 R_{22}. Further confirmation can be found in the height of the heat treatment damping peak of Fig. 7b. The observed reductions in height of this peak for the matrix in the axial and transverse specimens agreed with that predicted by the ROM and HT relations, respectively.

The above results and discussion imply that the ROM and HT relations can be employed to accurately predict axial and transverse dynamic properties provided exact phase dynamic properties are known. As has been discussed, this last requirement was difficult to fulfill for B/Al due to slight variations in phase properties. Nevertheless, by averaging these variations one can obtain good approximations for the boron fiber and aluminum matrix low strain dynamic modulus and damping capacity at 2000 Hz. These are given by the solid lines of Fig. 8. It should be noted that the time-temperature kinetics of the anelastic mechanisms responsible for the high temperature drop in modulus and rise in damping have been carefully studied both for the fiber (1) and the aluminum phase (7). With these kinetics it is possible to predict phase dynamic properties at other frequencies. The predictions for 0.2 and 20 Hz are also presented in Fig. 8. With this data, the ROM equation, and the HT equation, one can now obtain good estimates for the low strain axial and transverse dynamic properties of B/Al composites as a function of frequency (time), temperature, and fiber volume fraction. The effect of high strain vibration on the fiber dynamic properties has been discussed elsewhere (3).

Structure Evaluation

This preliminary study on the dynamic response of B/Al composites has revealed several areas where dynamic data of the flexural test could be of practical aid in determining environmental effects on composite and phase structures. For instance, dynamic modulus measurements have revealed a low stiffness for the M2 panel which can be interpreted as a problem in

fabrication conditions leading to poor fiber-matrix bonding. Because this bonding problem appears to translate directly into a loss of composite strength, the flexural test applied to low strength composites could serve to distinguish bonding effects from other weakening effects such as degraded fibers. The test also might aid in monitoring progressive fiber-matrix debonding caused for example by mechanical or thermal fatigue. It should be realized, however, that the modulus data are absolute measurements requiring accurate data on specimen mass, dimensions, and fiber volume fraction. Since bonding problems are indicated by non-agreement between measured and theoretical moduli, slight errors in specimen physical parameters could make definite conclusions impossible (see Table I). For this reason the sensitivity of the modulus measurement is greatly enhanced if the same specimen were examined before and after subjection to an environmental test.

The damping capacity ψ measurement is unlike the dynamic modulus measurement in two important ways. First, being a relative measurement it does not require any preliminary data concerning specimen mass or dimensions. Second, it is sensitive only to time-dependent deformation mechanisms within the composite macrostructure and phase microstructure. Thus if the damping of the constituent phases are known before composite fabrication, the composite damping can be a simple technique for monitoring and evaluating changes in phase microstructure caused by the composite environment. Because the phases may be affected differently, it is important to vibrate specimens in directions which accentuate as much as possible the damping contribution of each phase. Thus, for example, the

transverse B/Al data suggest that the 270° C composite damping peak observed after heat treatment was produced by a thermally-induced microstructural change within the 6061 aluminum matrix. The question whether this change may somehow be an indication of composite strength degradation has yet to be answered. Indeed the relatively weak M2 panel displayed this same damping structure in the as-fabricated condition. In any case, it appears that damping measurements near 270° C can be a practical tool for evaluating the thermal history of the matrix and thus of the B/Al composite.

CONCLUDING REMARKS

The proven success of the flexural vibration test described here should now permit easy acquisition of accurate temperature-dependent dynamic property data for any composite material in bar form. Because of the resonance requirement, test frequencies are fixed by the specimen dimensions and the tone number of the free-free flexural mode. Although low amplitude studies are necessitated by use of the electrostatic force and detection technique, measurement temperatures greater than 500° C can be achieved.

The availability of time-temperature dynamic data coupled with the predictive accuracy of composite theory implies a future potential for utilizing such data for the basic examination of environmental effects on composite macrostructure and microstructure. If this information can be correlated with variations in macroscopic properties, dynamic examination becomes a valuable tool for evaluation and prediction of gross composite behavior as a function of environmental conditions. Thus from the results

of this exploratory B/Al study, it is clear that future research must be performed to determine the practical significance of the observed changes in fiber-matrix bonding and in fiber and matrix microstructure which occurred during composite fabrication and use.

APPENDIX I

Frequency Constants

To account for rotary inertia and shear effects on the free-free flexural vibration of a uniform beam, Huang (6) has shown that the frequency constants b_n of Eq. (3) can be determined from a transcendental equation which includes the Timoschenko constant k and the modulus G for shear deformation transverse to the beam length. To solve this equation for beams with large ℓ/h ratios, one can make the first order approximation

$$b_n = b_n^o(1 + \lambda_n) \tag{31}$$

where $\lambda_n << 1$ and b_n^o are the solutions at zero beam thickness (Bernoulli-Euler theory). Substituting Eq. (31) into Huang's Eq. (36), one finds for the two lowest symmetrical tones that

$$b_1^o = 22.3733$$

$$\lambda_1 = \frac{r^2(24.74 + 6.15\ E/kG)}{1 + r^2(42.2 + 14.8\ E/kG)} \tag{32}$$

and

$$b_3^o = 120.9034$$

$$\lambda_3 = \frac{r^2(93.43 + 49.45\ E/kG)}{1 + r^2(170 + 104\ E/kG)} \tag{33}$$

For a beam with rectangular cross section, $r^2 = h^2/12\ell^2$ and $k = 5/6$ (Ref. 19).

The above formulas were found to yield b_n in excellent agreement with the exact b_n as long as $\lambda_n < 0.1$. Thus for rectangular beams with

$E/G < 4$ (such as 50 volume percent B/Al), Eq. (32) can be used to calculate b_1 for beams with $\ell/h > 6$ and Eq. (33) to calculate b_3 for beams with $\ell/h > 15$. Dudek (20) has discussed the frequency effects for composite beams with large E/G ratios.

APPENDIX II

Composite Flexural Modulus

The flexural dynamic modulus of a long specimen can be calculated from

$$E^b = \int_\Omega E^Y z^2 \, d\Omega \Big/ \int_\Omega z^2 \, d\Omega \tag{34}$$

where E^Y is the longitudinal dynamic Young's modulus for the volume element $d\Omega$ located a distance z above the neutral bend plane. To determine E^b for a unidirectional composite with fibers aligned within the plane of flexural vibration (axial mode), one can assume a rule-of-mixtures for the modulus E^Y of each composite layer of thickness dz. That is,

$$E^Y(z) = E_m + (E_f - E_m)\bar{v}_f(z)$$

where $\bar{v}_f$ is the effective volume fraction of fibers in the volume element $d\Omega = w\ell \, dz$. Using this approach for a composite with N identical plys each of thickness $\Delta h = h/N$, one finds from Eq. (34) that

$$E^b = E_{11} - (E_f - E_m)v_f P_N$$

where

$$P_N = [1 - 3d^2/4(\Delta h)^2]/N^2$$

Here v_f is the fiber volume fraction of the composite and d is the fiber diameter. Thus as ply number increases, E^b becomes essentially equal to E_{11}, the tensile modulus predicted by the rule-of-mixtures for uniaxial extension parallel to the fiber direction.

REFERENCES

1. DiCarlo, J. A., Scripta Metallurgica, Vol. 10, 1976, pp. 115-119.
2. DiCarlo, J. A., Composite Materials: Testing and Design (Fourth Conference), ASTM STP 617, American Society for Testing and Materials, Philadelphia, PA, 1977, pp. 443-465.
3. DiCarlo, J. A., Second International Conference on Composite Materials, The Metallurgical Society of AIME, April 1978.
4. Rosinger, H. E. and Ritchie, I. G., Journal of Testing and Evaluation, Vol. 2, No. 3, May 1974, pp. 131-138.
5. Cheng, Y. F., Fibre Science and Technology, Vol. 10, No. 1, 1977, pp. 23-25.
6. Huang, T. C., Journal of Applied Mechanics, Vol. 28, 1961, pp. 579-584.
7. Nowick, A. S. and Berry, B. S., Anelastic Relaxation in Crystalline Solids, Academic Press, New York, 1972.
8. Pagano, N. J., Composite Materials, Vol. 2, G. P. Sendeckyj, Ed., Academic Press, New York, 1974, pp. 1-22.
9. Hashin, Z., International Journal of Solids and Structures, Vol. 6, 1970, pp. 797-807.
10. Ashton, J. E., Halpin, J. C., and Petit, P. H., Primer on Composite Materials: Analysis, Technomic Publishing Co., Stamford, Conn., 1969, pp. 72-94.
11. Grimes, H. H., Lad, R. A., and Maisel, J. E., Second International Conference on Composite Materials, The Metallurgical Society of AIME, April 1978.
12. Grimes, H. H., Lad, R. A., and Maisel, J. E., Metallurgical Transactions A, Vol. 8A, 1977, pp. 1999-2005.

13. Metals Reference Handbook, C. J. Smithells, Ed., Butterworths, London, 1976.

14. Kreider, K. G. and Patarini, V. M., Metallurgical Transactions, Vol. 1, 1970, pp. 3431-3435.

15. Rizzo, H. F., Boron: Synthesis, Structure, and Properties, J. A. Kohn, Ed., Plenum Press, New York, 1960, pp. 175-189.

16. Metcalfe, A. G. and Klein, M. J., Composite Materials, Vol. 1, A. G. Metcalfe, Ed., Academic Press, New York, 1974, pp. 125-168.

17. Rieu, G.: Private communication.

18. Williams, K. J., Acta Metallurgica, Vol. 15, 1967, pp. 393-395.

19. Ritchie, I. G., Journal of Sound and Vibration, Vol. 31, 1973, pp. 453-468.

20. Dudek, T. J., Journal of Composite Materials, Vol. 4, 1970, pp. 232-241.

TABLE 1. - B/Al SPECIMEN PROPERTIES AT 22° C

Manufacturer (matrix alloy)	Average fiber volume fraction, %	Average matrix density, g/cm^3	Dynamic modulus at ∿2000 Hz, GPa		
			Experimental		Theory
			E_{11}	E_{22}	
M1 (6061)	50.4±0.7	2.60±0.02	249±3		244±5
M1 (6061)	52.0±0.7	2.64±0.03	248±4		252±5
M1 (6061)	51.4±0.7	2.60±0.03	249±3		247±5
M1 (1100)	48.5±0.9	2.62±0.03	247±5		237±6
M2 (6061)	46.7±0.8	2.64±0.04	219±5		231±5
M2 (6061)	46.7±0.8	2.64±0.04		138±7	154±3

TABLE 2. - B/Al PHASE PROPERTIES AT 22° C

	Density, g/cm^3	Dynamic modulus at 2000 Hz, GPa	Poisson's ratio	Coefficient of thermal expansion, $°C^{-1}$ (e)
Fiber: 203 μm boron on tungsten[a]	2.410	414±6[c]	0.13	5.0×10^{-6}
Matrix: 1100 or 6061 aluminum alloy[b]	2.70	69[d]	0.33	25.5×10^{-6}

[a]Reference 3.

[b]Reference 13.

[c]Elastic Young's modulus corrected for anelastic effects (-1 %).

[d]Estimated from the Voigt and Reuss averages of single crystal data.

[e]Average value between 20° and 300° C.

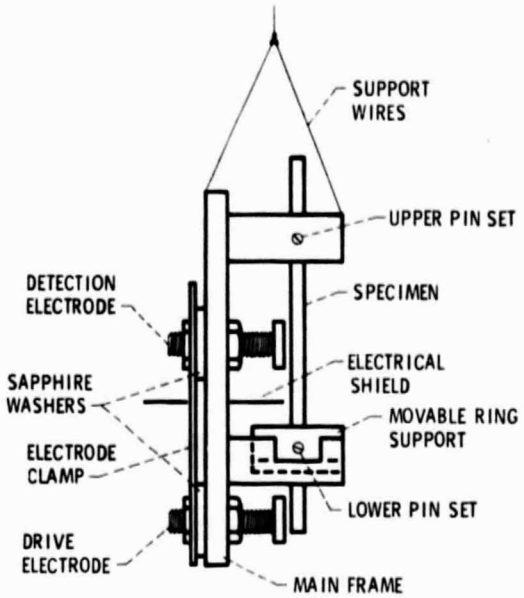

Figure 1. - Schematic of test rig for the forced vibration of composite bars at free-free flexural resonance.

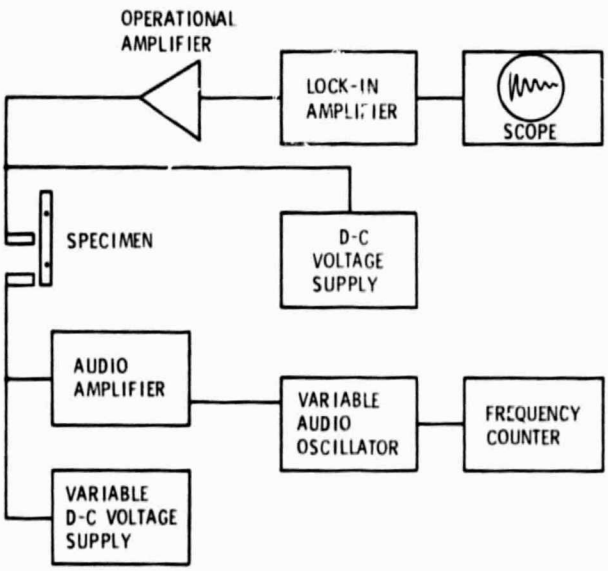

Figure 2. - Block diagram of the electrostatic drive and detection system.

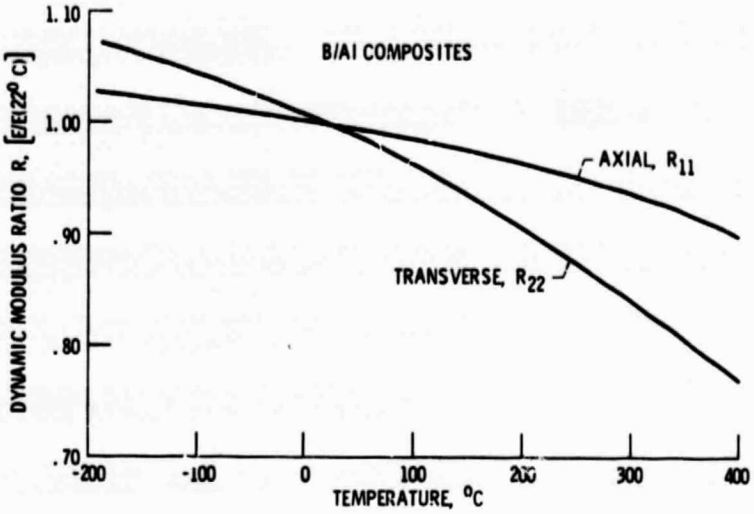

Figure 3. - Temperature dependence of the axial and transverse dynamic moduli of 50 vol. percent B/Al composites vibrating at low strain near 2000 Hz.

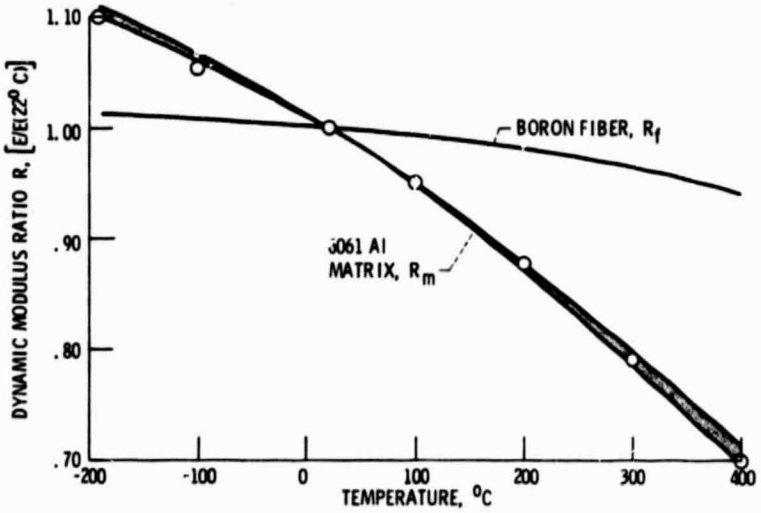

Figure 4. - Temperature dependence of the B/Al phase dynamic moduli for the B/Al phases vibrating at low strain near 2000 Hz. Fiber curve was obtained from measurements on single fibers (1). Matrix data points and curves were calculated from composite results for axial R_{11} and transverse R_{22}, respectively.

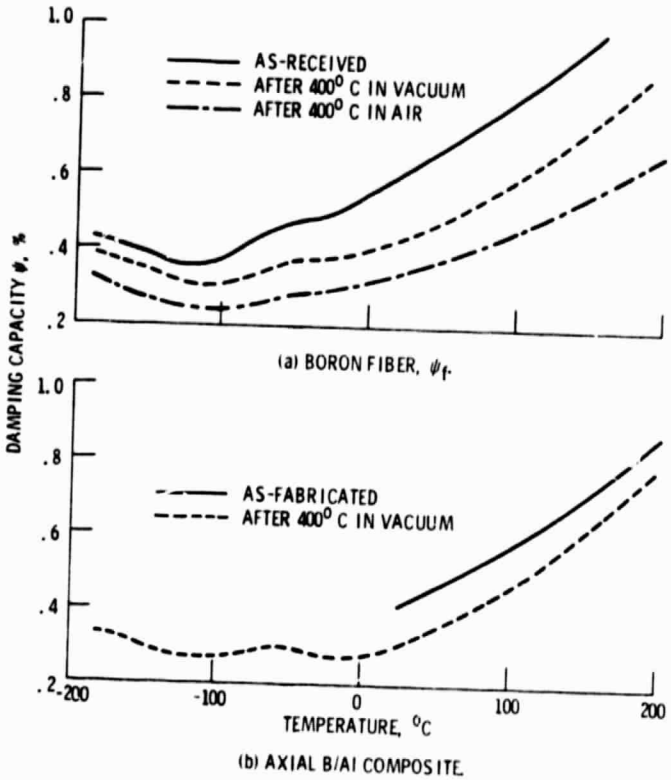

Figure 5. - Low temperature effects of heat treatment conditions on the damping capacity at low strain and ~2000 Hz.

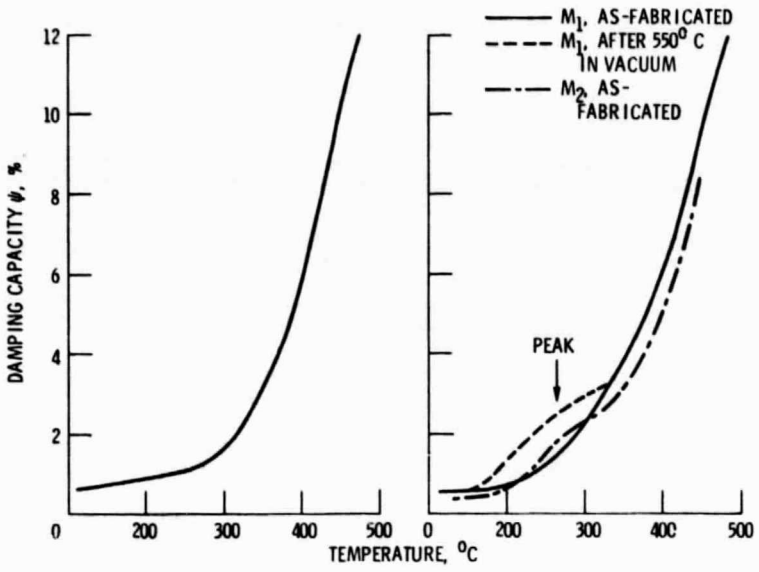

(a) BORON FIBER, ψ_f. (b) B/Al AXIAL COMPOSITES, ψ_{11}.

Figure 6. - High temperature effects of heat treatment conditions on the damping capacity at low strain and ~2000 Hz.

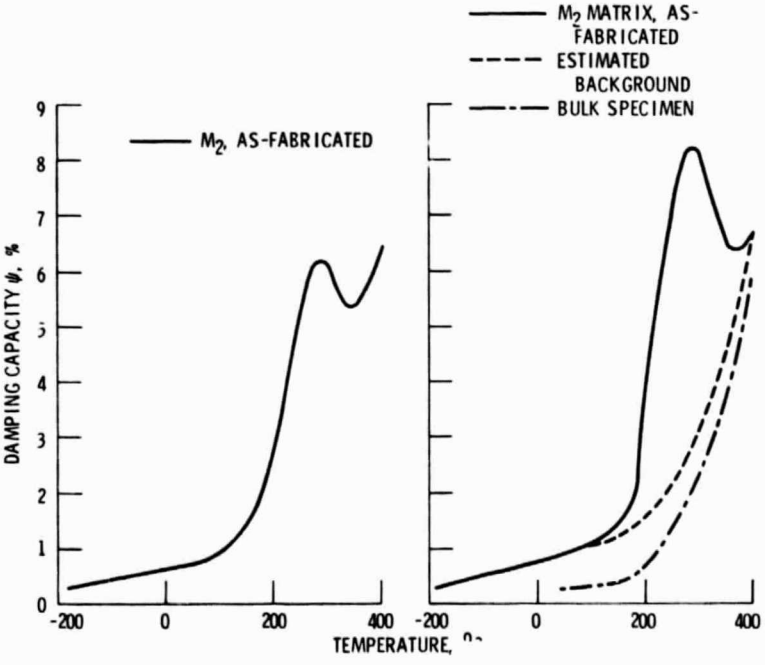

(a) TRANSVERSE B/Al COMPOSITE, ψ_{22}. (b) 6061 ALUMINUM, ψ_m.

Figure 7. - Temperature dependence of the damping capacity at low strain and ~2000 Hz.

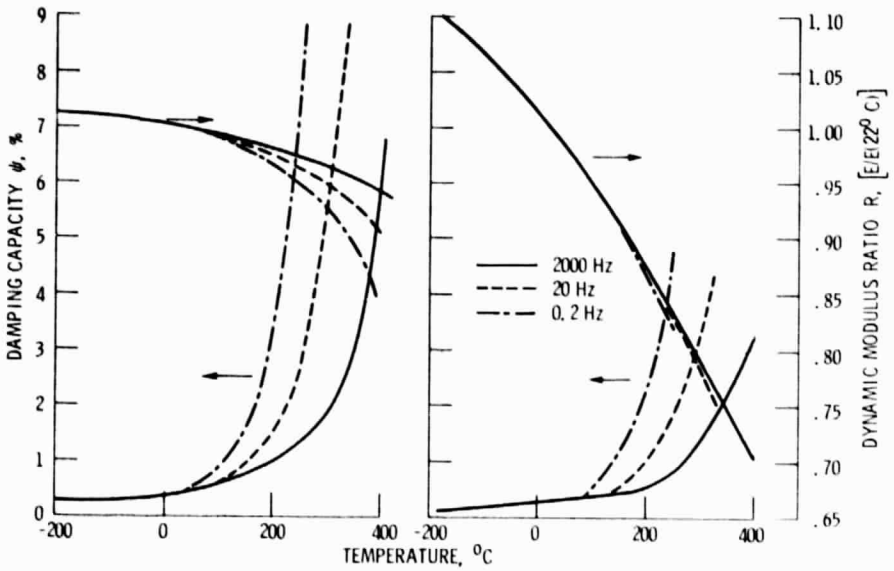

(a) BORON FIBER, $E(22^{o}\ C) \cong 414$ GPa.

(b) ALUMINUM MATRIX (6061), $E(22^{o}\ C) \cong 69$ GPa.

Figure 8. - Temperature and frequency dependence for the low strain damping capacity and dynamic modulus of boron fiber and aluminum matrix (6061 alloy).